SIMULATION OF THE THREE EDGE BEARING TEST: 3D MODEL FOR THE STUDY OF THE STRENGTH CAPACITY OF SFRC PIPES

Facundo L. Ferrado[a], Mario R. Escalante[a] and Viviana C. Rougier[a,b]

[a]*Grupo de Investigación en Mecánica Computacional y Estructuras, Universidad Tecnológica Nacional- Facultad Regional Concepción del Uruguay, Ing. Pereyra 676, 3260 Concepción del Uruguay, Argentina, gimce@frcu.utn.edu.ar*

[b]*Grupo de Investigación sobre Hormigones Estructurales, Universidad Tecnológica Nacional-Facultad Regional Concordia, Salta 277, 3200 Concordia, Argentina.*

Keywords: Concrete pipes, SFRC, non-lineal model, plasticity.

Abstract. The use of SFRC as building material, has been expanding its possibilities beyond conventional applications. Among its new applications, SFRC pipes appear as a new reliable alternative to the common pipes which use steel mesh as reinforcement, due to the structural benefits that mean the fiber addition. In spite of the advances achieved regarding the knowledge of the behavior of SFRC as a structural material, a numerical tool which allows to predict the mechanical response of SFRC pipes is needed, this is due to the complexity of the costly experimental campaigns. In this work the mechanical behavior of SFRC pipes is numerically assessed by means of the simulation of the three edge bearing test (TEBT) according to IRAM 11503 standard through a tridimensional model, which is implemented using a finite element analysis tool. SFRC is considered as an homogeneous material described for a damage-plasticity model which consider different behaviors in tension and compression by means of stress-strain uniaxial curves. These curves are obtained from equations arising from theoretical-experimental developments of other authors. Finally the results of the simulations are shown by means of load-deflection curves, ultimate loads charts and strength distribution diagrams, which are compared with those ones obtained in a experimental campaign carried out by the authors themselves. The results are complemented with some pictures depicting the experimental campaign mentioned above, with both the equipment used during the tests as well as the failure modes of the pipes are shown.

1 INTRODUCTION

As known, concrete is the most frequently used construction material, but it has inherent drawbacks, like low tensile strength, low ductility and low energy absorption. An effective way to overcoming these drawbacks of plain concrete is by adding a small fraction of discrete and shorts steel fibers to the concrete while mixing with aggregates and cement mass, giving place to a new composite material called steel fiber reinforced concrete (SFRC). Research on SFRC started in 1960s and nowadays it is widely accepted that such kind of concrete can significantly improve many behaviors of concrete. A most extensive literature review of the applications and the properties of SFRC could be seen in the work of Behbahani et. al. and Ahmad & Kapoor (Behbahani et al., 2011), (Ahmad and Kapoor, 2016).

An efficient application of SFRC in building structures such as concrete pipes allows to reduce the labor cost associated with reinforcement works, by means of partial of total substitution of rebar, besides providing a number of qualitative advantages such as higher durability, temperature resistance and water resistance (Kinash and Bilozir, 2015). Despite its extensive and long-term use in specific areas, e.g. industrial floors, steel fibres have not occupied the general market of concrete structures. One of the main reasons is that the major design codes do not consider SFRC structures and, in addition, the absence of material models of SFRC reliable for numerical analysis makes that application fields of this material are still limited (di Prisco et al., 2013).

Generally, SFRC can be considered as a homogeneous material, it means conventional concrete with improved material properties. Modelling SFRC as a concrete with randomly dispersed fibres could involve a large number of generally stochastic parameters and for that reason such models tend to be very complex and consequently time consumming. So, nowadays most of the models found in literature propose simple and continuous non-differentiable constitutive diagrams that are characterised through macroscopic material properties. These approaches focus either on stress-strain relationships ($\sigma - \epsilon$) or stress-crack opening width ($\sigma - w$) relationships (Meskenas et al., 2014).

2 EXPERIMENTAL PROCEDURE

An experimental campaign has been carried out in order to evaluate the SFRC performance as total or partial replacement of the traditional steel mesh reinforcement. For that purpose, both concrete pipes reinforced with steel mesh and with steel fibers were cast and tested. Until now, two pipes with a steel mesh class III according to the standard IRAM 11503, two with SFRC containing a fiber dosage of $20\,\text{kg/m}^3$ (mix 1) and two with SFRC containing a fiber dosage of $25\,\text{kg/m}^3$ (mix 2) were produced. WIRAND® FF1 low carbon steel fibers with hooked ends were used which have 50 mm of length and a diameter of 1 mm. All pipes has a internal diameter of 600 mm, external bell diameter of 897 mm, wall thickness of 75 mm and a length of 1000 mm and they were produced in a single day in order to avoid the influence of the intervening variables in their production. The designation used for the different pipes and their reinforcement are summarized in Table 1. Concrete properties such as uniaxial compression strength (σ_c) and uniaxial tension strength (σ_t) were obtained from cylindrical specimens tests, meanwhile flexure tests of notched beams (150 x 150 x 550 mm) were performed for obtaining of fracture energy (G_f). All these material properties are necessary in the formulation of the numerical model. More details about the experimental campaign are omitted here since it is not the object of study in the present work.

Pipe Designation	Reinforcement	Fiber Dosage (kg/m^3)
T1M	Steel mesh IRAM Class III	-
T2M	Steel mesh IRAM Class III	-
T1F20	-	20
T2F20	-	20
T1F25	-	25
T2F25	-	25

Table 1: Fabricated 600 mm diameter pipes.

2.1 The three edge bearing test procedure

The three edge bearing test consists of a diametral compression test which is used to classify concrete pipes in different strength classes. The test is described in the IRAM 11503 standard and consists in a line load that is applied along the crown of the pipe using an universal displacement controlled testing system. In Figure 1 can be seen an image of the machinery used with a pipe ready to be tested.

Figure 1: Three edge bearing test set up. Left: schematics cross sectional view. Right: side view.

The vertical and horizontal deflection were measured in both ends of the pipes. For this purpose four dial and digital gauges with a precision of 0.001 mm were used. The ultimate loads achieved for each one of the tested pipes and the vertical displacements measured are summarized in the Table 2.

Pipe Designation	Ult. Load (kg)	Spigot Displ. (mm)	Bell Displ. (mm)
T1M	7000	1.17	0.47
T2M	8000	2.10	0.90
T1F20	5700	0.68	0.36
T2F20	6400	1.25	0.21
T1F25	6900	1.40	0.56
T2F25	7000	1.20	0.38

Table 2: Ultimate load values and displacement measured in the tested pipes.

3   NUMERICAL MODEL

In this section, the main aspects of the tridimensional model adopted for the simulation of the TEBT is presented, through which the mechanical behaviour of the pipes is numerically assessed. Previously, the authors have been studying the problem with a bidimensional model in plain strain state (Ferrado et al., 2015) , (Ferrado et al., 2016). This model is computationally implemented in the finite element analysis software ABAQUS. Following, the constitutive model adopted for concrete is described.

3.1   SFRC modelling: Concrete Damaged Plasticity Model

The Concrete Damaged Plasticity (CDP) model is used to represent the behavior of the concrete. It assumes that the main two failure mechanisms are tensile cracking and compressive crushing of the concrete material. Thus, the model consider different behaviours under this two solicitations. Under uniaxial tension the stress-strain response is linear elastic until the value of the failure stress is reached. Beyond the failure stress the formation of micro-cracks is represented macroscopically with a softening stress-strain response.

On the other hand, under uniaxial compression the response is linear until the value of initial yield. In the plastic regime the response is typically characterized by stress hardening followed by strain softening beyond the ultimate stress. Figure 2 shows the typical response of the concrete under uniaxial tension and compression according to the CDP model.
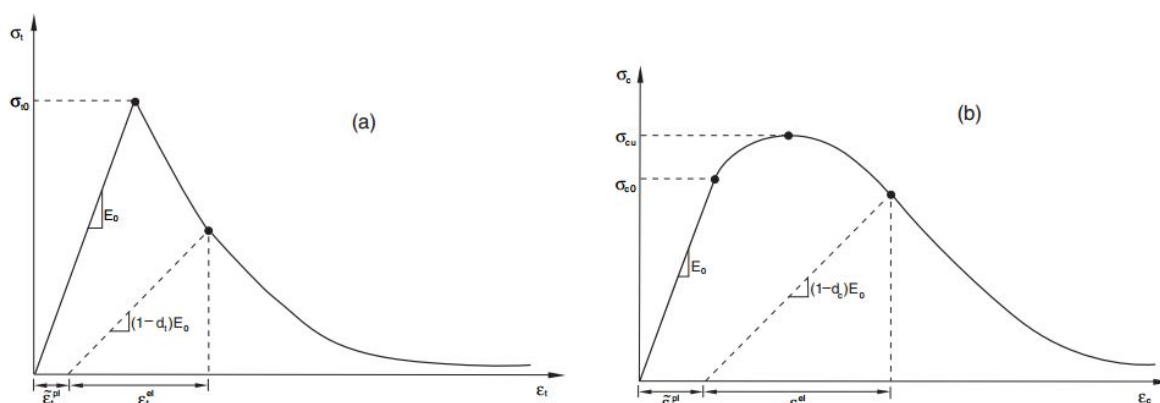
Figure 2: Concrete response under uniaxial loads. Left: uniaxial tension. Right: uniaxial compression.

This representation, although somewhat simplified, captures the main features of the response of concrete. A more detailed description of this model can be found in the already mentioned work (Ferrado et al., 2016). The plasticity parameters adopted are detailed in Table 3.

Parameter	Dilation Angle	Viscosity	Excentricity	σ_{co}/σ_{bo}	K_c
Value	36.31º	0	0.1	1.16	0.67

Table 3: CDP model plasticity parameters.

3.2 Uniaxial compression and tension behavior of SFRC

Then, to represent the behavior of the SFRC, the uniaxial stress-strain curves for compression and tension are defined. With regard to the compression behavior, a model proposed by Barros and Figueiras is used (Barros and Figueiras, 1999). The stress-strain relationships have the following expressions:

$$\sigma = f_{cf} \frac{\frac{\epsilon}{\epsilon_{pf}}}{(1-p-q) + q(\frac{\epsilon}{\epsilon_{pf}}) + p(\frac{\epsilon}{\epsilon_{pf}})^{\frac{(1-q)}{q}}}, \tag{1}$$

with

$$q = 1 - p - \frac{E_{pf}}{E_c}, \ p + q \in [0,1] \ \text{and} \ \frac{1-q}{p} > 0, \tag{2}$$

$$E_{pf} = \frac{f_{cf}}{\epsilon_{pf}} \ \text{and} \ E_c = 0.043.2400^{1.5}.\sqrt{f_c} \ \text{(CIRSOC 201)} \tag{3}$$

where f_c is the characteristic compression strength of the mix. For hooked end fibers with dimensions of: length: 60mm, diameter= 0.8 mm , slenderness: 75 we have:

$$\epsilon_{pf} = \epsilon_{co} + 0.00026 W_f \quad p = 1 - 0.722 e^{-0.144 W_f} \tag{4}$$

where ϵ_{co} is the strain for the maximum concrete stress (ϵ_{co} = 0.0021 for the strength class of the concrete used here according to FIB Model CODE 2010). Figure 3 shows the stress-strain curves in compression used in the CDP model.
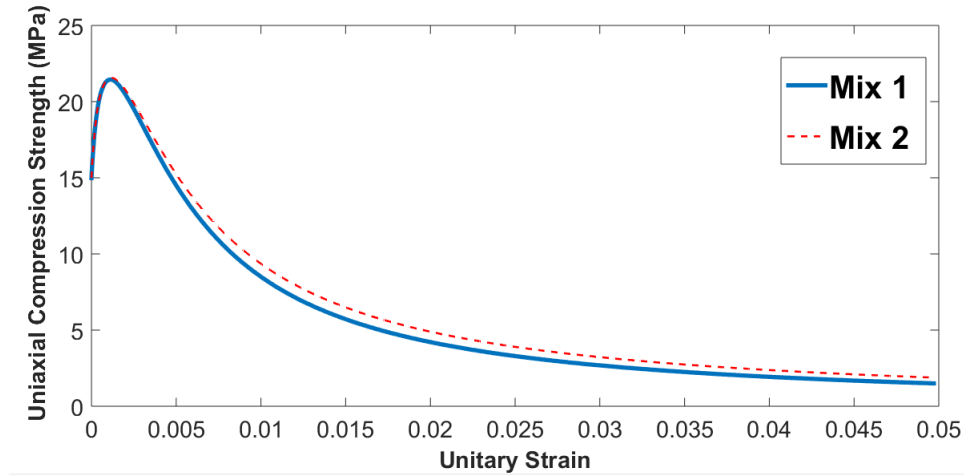
Figure 3: Compression stress-strain curves for SFRC used in the CDP model.

To modelling the tension behavior a methodology developed by Amin et. al. (Amin et al., 2015) is used. These authors propose a derivation of the stress-strain relationship by means of a indirect method resorting to a flexural test executed on prismatic beams. According to this methodology, the authors argue that the strength of the composite, in function of the crack opening (w) has two components:

$$\sigma(w) = \sigma_c(w) + \sigma_f(w) \tag{5}$$

where σ_c (w) is the contribution of the concrete matrix, meanwhile that σ_f (w) is the component that belongs to the fibers.

For common concrete, the tensile strength could be consider as (Voo and Foster, 2004), (Voo and Foster, 2009), (Lee and Foster, 2008):

$$\sigma_c(w) = c_1 \, f_{ct} \, e^{-c_2 w} \tag{6}$$

where c_1 is a coefficient that take into account the positive effects of the fibers on the maximum strength of the matrix, and c_2 is a factor that controls the slope of the descending branch of the curve $\sigma - w$ which is influenced for the fiber dosage and the composition of the cementitious matrix. Voo and Foster (Voo and Foster, 2004), (Voo and Foster, 2009), (Voo and Foster, 2003) adopt the value of c_1 equal to the unity and for c_2 Ng et. al. (Ng et al., 2012) proposed the following:

$$c_2 = \frac{20}{1 + 100.V_f} \tag{7}$$

where V_f is the fiber dosage of the mix. The tensile strength can be estimated from the compression strength by the formula: $f_{ct} = 0.6.\sqrt{f_{cf}}$ (Voo and Foster, 2003).

To take into account the contribution of the fibers, Voo and Foster (Voo and Foster, 2003) use a concept that they called fiber engagement length, by which they infers that in a composite material which contains fibers randomly oriented, exists an critical angle for which the fibers becomes active. Considering this concept and others regarding with the fiber dosage that probabilistically across a crack plane together with the geometry of them, it is reached the following expresion:

$$\sigma_f(w) = \frac{1}{\pi}.\arctan(\frac{w}{\alpha}).(1 - 2\frac{2w}{l_f})^2.\frac{l_f}{d_f}.V_f.\tau_b \tag{8}$$

where α corresponds to a fiber anchorage parameter, which for hooked end fibers is given by: $\alpha = d_f/3.5$ (Voo and Foster, 2003).

Finally, τ_b is the mean shear stress between the fibers and the matrix and can be taken as $0.8.\sqrt{f_c}$ (Gouveia et al., 2014). Based on this formulations and the data obtained experimentally, the stress-strain curves used in the numerical model are obtained. Figure 4 shows the curves for the concrete mixes studied here.
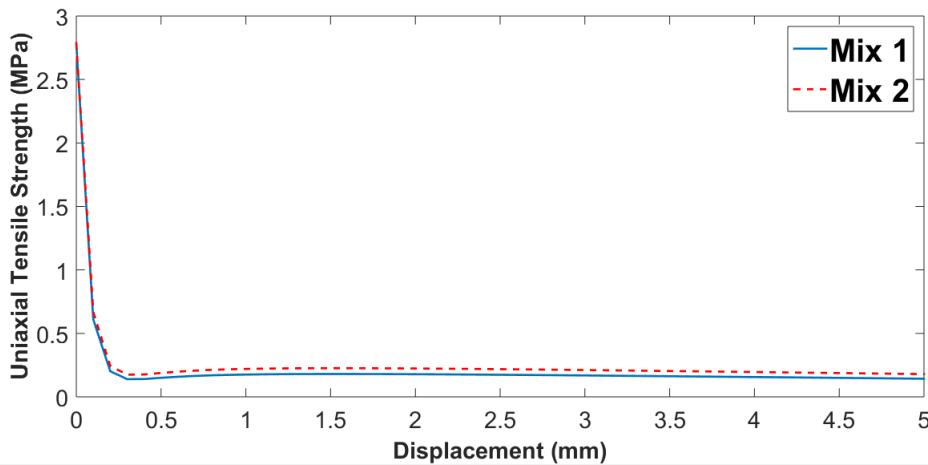
Figure 4: Tension stress-strain curves for SFRC used in the CDP model.

3.3 Numerical Simulation of the Three Edge Bearing Test

The geometry consists of the upper loading strip, lower supporting strips, and the concrete pipe. The upper and lower strips had dimensions of 50 mm weight and 30 mm height and the lower bearing strips were 50 mm apart following the requirements of the IRAM 11503 standard. For the mesh, 8-node linear brick with reduced integration elements were used (C3D8R). Displacement controlled loading was accomplished by applying a downward displacement at the upper bearing strip. The two lower bearing strips served as supports and were fixed at the bottom to prevent rotational or translational degrees of freedom. The interaction between the pipe and the upper and lower strips was modeled using a simple tie constraint. The standard IRAM 11503 specifies that the supports must be rubber strips with a Shore hardness of 50 ± 5. Thus, it is proposed the use of a semi-empiric formula developed by Gent (Gent, 1958) and used later by others authors (Methtananda et al., 2009) that establish a relationship between the Shore hardness and the Young modulus. The expression that relates these two parameters is the following:

$$E\,(\text{Mpa}) = \frac{0.0981.(56 + 7.66.S)}{0.137505.(254 - 2.54.S)} \tag{9}$$

where S is the Shore hardness.

So, for a value of Shore hardness of 50 a Young Modulus of 2.46 Mpa is obtained. Rubberlike materials (and other elastomeric materials) are modeled, in the most basic sense, as hyperelastic, that is, as non-linear elastic. An analysis of a rubber material as elastic is not appropriate since it can not deal with the capabilities of this type of materials such as large deformations leading to poor results. The hyperelastic model of Neo-Hooke is used here, which is one of the simplest models to treat hyperelasticity. This model is an extension of the Hooke law for the case of large deformations and is applicable for certain plastics and also for elastomers as we have here. Hyperelastic materials are described in terms of "Strain energy density function" which is defined as the deformation energy per unit volume. The strain energy density function for an incompressible Neo-Hookean material is given by:

$$W = C_{10}.(I_1 - 3) \tag{10}$$

where C_{10} is a temperature-dependent material parameter and I_1 is the first deviatoric strain invariant (ABAQUS Analysis User's Guide Volume III: Materials). In this formulation the shear modulus is given by:

$$\mu = 2.C_{10} \tag{11}$$

For incompressible materials, the Poisson ratio is ≈ 0.5. So, for E = 2.46 Mpa and $\nu \approx 0.5$ we have: $\mu = 0.82$. From Eq. (11) we obtain $C_{10} = 0.41$. The Neo-Hookean model for hyperelastic materials included in ABAQUS requires the definition of another material parameter D_1 which is 0 for incompressible materials.

The densities of the concrete and the rubber materials were also defined since the problem was solved by a dynamic (quasi-static) analysis. Dynamic type analysis require a "time períod" in seconds to apply the load, which was set at 900 seconds since experimentally the test of a pipe lasts about 15 minutes. In addition, a maximum number of 100 time increments and a minimum increment size of 0.009 was adopted as parameters to ending the analysis. So, the analysis will terminate when either value is crossed. The Figure 5 shows the load-deflection curves obtained numerically for both mixes. To graph the curve, the total reaction of the supports (equivalent to the total load) and the strain of the inner of the pipe were numerically obtained. As can be
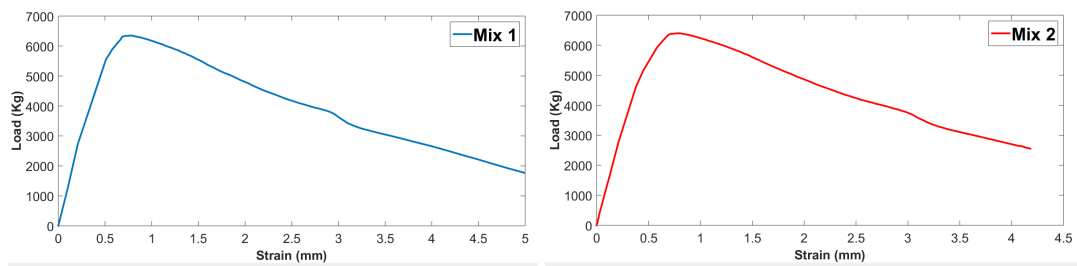
Figure 5: Numerical load-deflection curves. Left: mix 1. Right: mix 2.

seen, the model is capable to reproduce the elastic stage and the post-cracking stage of the load process, where a softening phenomena is observed for the SFRC mixes modelled here. Then, to validate the model, a comparison of the numerical results with the experimental ones was performed. For that purpose, the experimental and numerical load-deflection curves are plotted on the same graph. Figure 6 and 7 shows these comparisons.
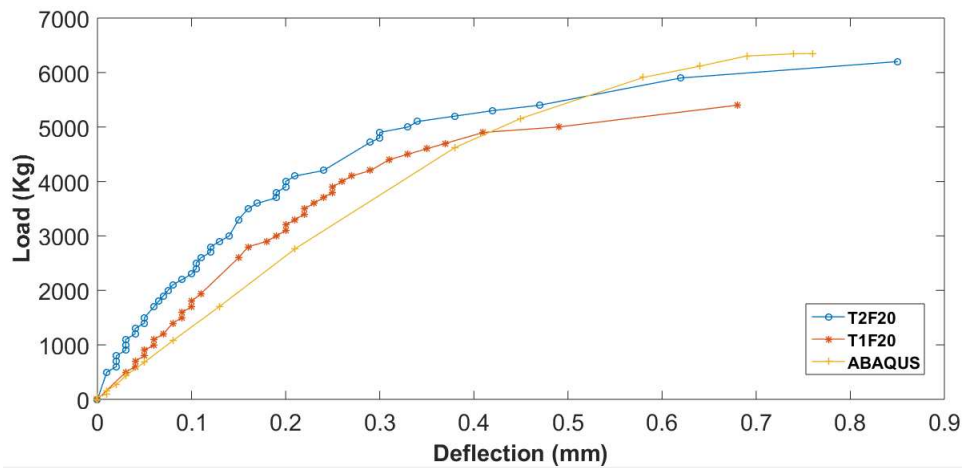
Figure 6: Numerical and experimental load-deflection curves for mix 1
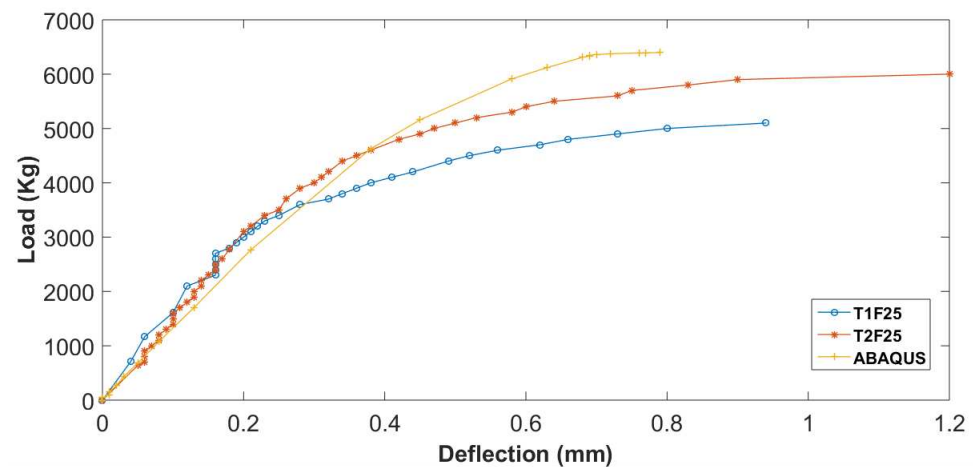
Figure 7: Numerical and experimental load-deflection curves for mix 2

It is mentioned that the measuring devices were removed before the maximum load was reached to preserve them, and for that reason the load values shown in those figures corresponds

to the last value for which the displacements are known. The ultimate loads values and the strain at maximum load are shown in Tables 4 and 5

Pipe Designation	Ultimate Load (Kg)	Displacement (mm)
T1F20	6400	0.95
T2F20	5700	0.68
ABAQUS	6347	0.76

Table 4: Ultimate load and vertical deflection values for mix 1

Pipe Designation	Ultimate Load (Kg)	Displacement (mm)
T1F25	6900	1.2
T2F25	7000	1.4
ABAQUS	6390	0.79

Table 5: Ultimate load and vertical deflection values for mix 2

As observed, there is an acceptable correlation between the values and diagrams obtained numerically and experimentally. However, it should be mentioned that the maximum loads and deflection values corresponding to these maximum loads obtained numerically are very similar for both mixtures, but experimentally higher load values were observed for the mixture with higher fiber content (mix 2), so that we could say that the proposed model underestimates the contribution of fibers for higher fiber contents. Finally, in the Figure 8 a stress distribution diagram of the maximum principal stresses is shown together with an image of a cracked pipe.
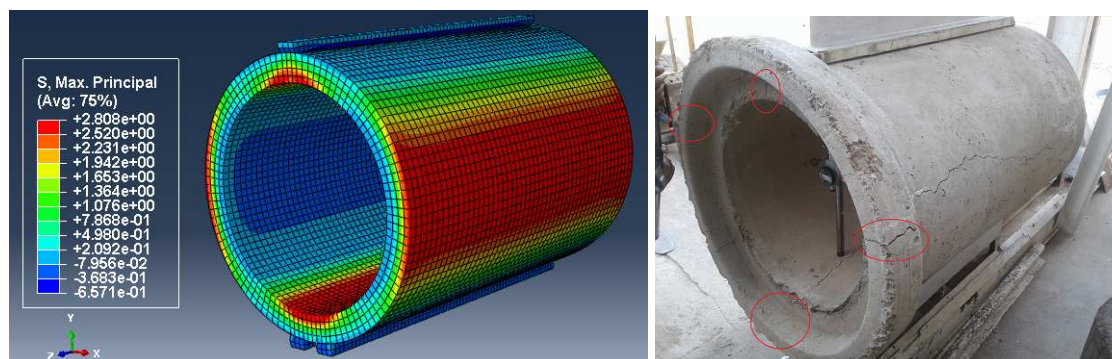
Figure 8: Left: maximum principal stresses diagram. Right: Typical flexure cracks on a tested pipe

From the figure it can be seen that the model represents the stress distribution properly since the sectors of the pipe in which the cracks appear during the experimental tests coincide with those in which the maximum principal stresses are numerically obtained (red coloured areas).

4   CONCLUSIONS

In this work, a tridimensional model of the TEBT for assesing the mechanical behavior of concrete pipes was presented. The model was implemented in the finite element method analysis tool ABAQUS where the SFRC was modeled as a homogenous material whose behavior was described through uniaxial tension and compression curves that were obtained through theoretical formulations proposed by other authors. Besides, a comparison of these results with the experimental ones obtained from a experimental campaign carried out for the authors themselves was performed. The model shown a good agreement for the both mixes regarding the

stress distribution and the shape of the load-deflection curves in comparison with the experimental results, but respecting the maximum loads achieved, the difference between the numerical and experimental values is more marked for the mix 2, so possibly the model proposed underestimate the contribution of fibers for high fiber contents. As a later stage it is suggested to elaborate pipes with higher fiber dosages and validate the model for these dosages.

REFERENCES

Ahmad E. and Kapoor E. A review study on use of steel fiber as reinforcement material with concrete. *International Journal of Latest Research in Science and Technology*, 5:37–39, 2016.

Amin A., Foster S., and Muttoni A. Derivation of the σ-w relationship for sfrc from prism bending tests. *Structural Concrete*, 16:93–105, 2015.

Barros J. and Figuieras J. Flexural behavior of sfrc: Testing and modeling. *Journal of Materials in Civil Engineering*, 11:331–339, 1999.

Behbahani H., Nematollahi B., and Farasatpour M. Steel fiber reinforced concrete: A review. In *Proceedings of the International Conference on Structural Engineering Construction and Management (ICSECM2011)*. 2011.

di Prisco M., Colombo H., and Dozio D. Fibre-reinforced concrete in fib model code 2010: principles, model and test validation. *Structural Concrete*, 14:342–361, 2013.

Ferrado F., Escalante M., and Rougier V. Modelacion numerica del comportamiento mecanico de tubos de hormigon reforzado con fibras de acero. *Proceedings of the XXXVI Iberian Latin-American Congress on Computational Methods in Engineering CILAMCE 2015*, 2015.

Ferrado F., Escalante M., and Rougier V. Numerical simulation of the three edge bearing test of steel fiber reinforced concrete pipes. *Mecanica Computacional*, XXXIV. Solid Mechanics (A):2329–2341, 2016.

Gent A. On the relation between indentation hardness and young's modulus. *Rubber Chemistry and Technology*, 31:896–906, 1958.

Gouveia N., Fernandes N., Faria D., Ramos A., and Lucio V. Sfrc flat slabs punching behaviour-experimental research. *Composites: Part B*, 63:161–171, 2014.

Kinash R. and Bilozir V. Deformational calculation method of bearing capability of fiber concrete steel bending elements. *Technical Transactions*, 111:49–58, 2015.

Lee G. and Foster S. Modelling of shear-fracture of fibre reinforced concrete. *Proceedings of International fib Symposium, Taylor Made Concrete Structures*, 2008.

Meskenas A., Gribniak V., Kaklauskas G., Arnautov A., and Rimkus A. Simplified technique for constitutive analysis of sfrc. *Journal of Civil Engineering and Management*, 20:446–453, 2014.

Methtananda I., Parker S., Patel M., and Braden M. The relationship between shore hardness of elastomeric dental materials and young's modulus. *Dental Materials*, 25:956–959, 2009.

Ng T., Htut T., and Foster S. Fracture of steel fibre-reinforced concrete - the unified variable engagement model. Technical Report, School of Civil & Environmental Engineering, The University of New South Wales, Australia, 2012.

Voo J.Y. and Foster S. *Variable engagement model for fibre reinforced concrete in tension*. Univ. of New South Wales, School of Civil and Environmental Engineering Sydney, 2003.

Voo J.Y. and Foster S. Tensile fracture of fibre reinforced concrete variable engagement model. *Proceedings of 6th Rilem Symposium on Fibre-reinforced Concrete*, 96:875–884, 2004.

Voo J.Y. and Foster S. *Reactive powder concrete: analysis and design of RPC girders*. Lambert Academic Publishing, 2009.